

Article

# Graphene Oxide Aerosol Deposition and its Influence on Cancer Cells. Preliminary Results

Barbara Nasiłowska <sup>1,\*</sup>, Zdzisław Bogdanowicz <sup>2</sup>, Kinga Hińcza <sup>3</sup>, Zygmunt Mierczyk <sup>1</sup>, Stanisław Góźdź <sup>4,5</sup>, Małgorzata Djas <sup>6</sup>, Krystian Kowiorski <sup>6</sup>, Aneta Bombalska <sup>1</sup>, and Artur Kowalik <sup>3,7</sup>

<sup>1</sup> Institute of Optoelectronics, Military University of Technology, gen. S. Kaliskiego 2, 00-908 Warsaw, Poland; zygmun.mierczyk@wat.edu.pl (Z.M.); aneta.bombalska@wat.edu.pl (A.B.)

<sup>2</sup> Faculty of Mechanical Engineering, Military University of Technology, gen. S. Kaliskiego 2, 00-908 Warsaw, Poland; zdzislaw.bogdanowicz@wat.edu.pl

<sup>3</sup> Department of Molecular Diagnostics, Holy Cross Cancer Center, Kielce, S. Artwińskiego 3, 25-735 Kielce, Poland; Kinga.Hincza@onkol.kielce.pl (K.H.); Artur.Kowalik@onkol.kielce.pl (A.K.)

<sup>4</sup> Department of Clinical Oncology, Holy Cross Cancer Center, Kielce, S. Artwińskiego 3, 25-735 Kielce, Poland; Stanislaw.Gozdz@onkol.kielce.pl

<sup>5</sup> Department of Prophylaxis and Cancer Epidemiology, Collegium Medicum, Jan Kochanowski University, Al. IX Wieków Kielc 19A, 25-317 Kielce, Poland

<sup>6</sup> Łukasiewicz Research Network—Institute of Electronic Materials Technology, Department of Chemical Synthesis and Flake Graphene; Wólczyńska 133, Warsaw 01-919, Poland; malgorzata.djas@itme.edu.pl (M.D.); krystian.kowiorski@itme.edu.pl (K.K.)

<sup>7</sup> Division of Medical Biology, Institute of Biology Jan Kochanowski University, Uniwersytecka 7, 25-406 Kielce, Poland

\* Correspondence: barbara.nasilowska@wat.edu.pl

Received: 14 September 2020; Accepted: 6 October 2020; Published: 8 October 2020



**Abstract:** This paper presents the results of the interaction of graphene oxide (GO) on MDA-MB-231 and SW-954 cancer cell lines. The tests were carried out in two variants. In the first one, GO was sprayed on a Petri dish and then, the cancer cell lines were cultured. In the second variant, the cells were covered with an aerosol containing GO. In both variants, cancer cell lines were incubated and tested every 24, 48, and 72 h. After each time period, cell viability and surface morphology were measured. The tests after 72 h showed that coating with GO aerosol caused a reduction in cell viability by 52.7% and 26.4% for MDA-MB-231 and SW-954 cancer cell lines, respectively, with respect to a reference sample (without the influence of GO aerosol). Tests where GO is a culture medium demonstrated a decrease in cell viability by approximately 4.3% compared to a reference sample for both considered cell lines.

**Keywords:** graphene oxide; cancer cells; GO aerosol; deposition

## 1. Introduction

Since 2010, when A. Geim and K. Novoselov were awarded a Nobel Prize in physics for graphene discovery, a great deal of research has been carried out concerning graphene and its derivatives [1]. Researchers have searched for different graphene applications in electronics [2–5], informatics [6], construction [7], material engineering [8–13], mechanics [10], medicine [11], and even sport [12].

Up to this day, numerous methods of graphene, reduced graphene oxide (rGO), and graphene oxide (GO) deposition have been developed. One of the most effective is chemical vapor deposition (CVD) [14–17]. One interesting method of thin layer deposition is the spray method. The first to examine and develop this method were Do-Yeon Kim et al. [18]. They presented supersonic kinetic spraying as

a method for rGO deposition on any kind of substrate. Graphene deposition with the use of this method turned out to be less complicated, more economical, and allowed large-scale graphene deposition [18]. Some papers reported graphene and GO deposition in terms of corrosion resistance [19,20] properties and improvement of electric [21] and material [22] properties. When analyzing medical applications of graphene, one can find reports about cell [23] and bacterial cytotoxicity [24,25].

Sengupta et al. [25] showed GO and rGO influence Gram-positive and Gram-negative bacteria. They reported that graphene/graphene oxide (G/GO) antibacterial activity depends on size, shape, and the kind of bacteria examined. GO was found to be more effective due to its oxygen functional groups. GO showed the ability to suppress cellular growth by inducing oxidative stress which destabilizes cell membranes and leads to cytoplasm leakage [25–27].

Jaworski et al. [28] reported results concerning the influence of graphene platelets (GPs) on the morphology and viability of glioma cells. It was found that graphene is toxic to glioma cells and induces apoptosis in the U188 cell line. No necrosis was reported. Glioma cells have the highest degree of malignancy, migrate intensely and fast, and spread fast in brain tissues. It was observed that the cytotoxic effect was proportional to the graphene concentration. Microscopic studies showed that graphene platelets (GPs) adhered to the cells, forming a thin and impermeable layer. This layer surrounds the body of the glioma cells, separates them from the extracellular environment, blocks the transport of various substances into the cell, and influences respiratory processes.

Tabish T.A. et al. [29] presented the results of functionalized graphene oxide, which during decomposition, adsorbed the enzymes responsible for invasiveness and tumor metastasis formation. Due to the cationic and hydrophilic residues of GO, enzymes such as Cathepsin D and Cathepsin L (CathD and CathL) were bound on the GO surface. Additionally, Tabish et al. found that the GO interaction led to the apoptosis of cancer cells. Wang X. et al. [30], in their publication, investigated the effect of GO on the ability of glioblastoma stem-like cells (GSCs) to form spheres, cell divisions, viability, and differentiation. They found that GO inhibits cell division and the formation of cell spheres through epigenetic mechanisms responsible for cell differentiation, reducing their ability to proliferate. Pei et al. [31] proved that GO nanoparticles are not toxic to cells, but the addition of PEGylated nano-graphene oxide to cisplatin (Pt) and doxorubicin (DOX) anticancer drugs resulted in apoptosis and necrosis of cancer cells, but also in a reduction in tumor size in vivo.

In the recent literature, inconsistent results are described concerning the influence of graphene and its derivatives on cells and tissues [32]. Some indicate biocompatibility [33,34] and others report that graphene flakes can cut through cells and damage them [35–37].

Undoubtedly, GO cannot be treated as the same kind of material. Their properties depend on three basic parameters: the number of graphene layers, surface development, and relation of carbon to oxygen atoms [38,39]. The fabrication method of graphene and its derivatives is crucial. Results presented by Jaworski and colleagues [40] showed that rGO, as compared to GO, showed a higher toxic effect on cancer cells. The authors point out that biocompatibility can be influenced by the purity of graphene after fabrication [40] and its concentration [39,40].

Interesting results were presented by Zhu Y. and coworkers [35]. They reported that cell membrane damage of human keratinocytes, epithelium lung cells, and murine macrophages progressed along the irregular edge of graphene flakes or sharp edges.

Such properties are the result of graphene structure, mainly sharp edges, when graphene or GO flakes are applied. Sharp edges cause physical damage to the cell membrane, which results in loss of membrane integrity and the leakage of intracellular content leading to its death.

The question occurs as to what kind of influence GO has on cancer cells. In the literature, the hypothesis that GO deposited on the cell surface can snip cell off air and nutrients leading to apoptosis is also described.

Due to its high surface oxygen content, GO causes oxidative stress and in this way, induces cellular death [36].

Inspired by the diversity and complexity of the problems described by these authors, it was attempted in this study to deposit GO in aerosol form on breast and vulva cancer cells and to process their culture. The results in the literature were compared with those described below. Selected cancer cell lines were cultured on a Petri dish with GO deposited on it. The authors realize that results indicating lowering the cancer cells' viability have tremendous significance in oncology focused on GO deposition in a form of aerosol.

The application of GO in oncology gives new possibilities in anticancer treatments. To the best of our knowledge, there is no other report dealing with GO spray and its influence on cancer cells. This article, therefore, presents insight into the possibility of new methods for cancer treatment.

## 2. Methodology

The experiments, aiming to examine the influence of GO on breast and vulva cancer cells, were carried out in two variants and control:

1. GO was deposited on the plasma cleaned Petri dish and then, it was subject to a vacuum drying process. The next step was sterilization with UV rays. The authors developed a procedure of depositing the GO on the glass. In that procedure, GO was sprayed under pressure, and then, it was subjected to vacuum drying at a temperature of 150 °C (Figure 1a).
2. The plasma cleaned Petri dish was exposed to UV rays as a sterilization process. MDA-MB-231 and SW-954 cancer cell lines were cultured on a prepared Petri dish and then, coated with GO in the form of an aerosol (Figure 1b).
3. The reference samples (control) were made similar to variant II for both cell lines, but without the final stage of the GO deposition. The Petri dish was plasma cleaned, subjected to UV radiation for sterilization, and then, the cell culture procedure was performed as it was described in Section 2.3.

A comparative analysis was also carried out with respect to the control sample (control, Figure 1c). The control sample included all procedures performed for variant I and II (plasma cleaning, UV sterilization, and cell culturing) except GO deposition. In the first step of preliminary sample preparation, all Petri dishes were subjected to surface cleaning by plasma reaction for 60 min with a plasma power of 100 W (SPI Supplies Plasma Prep III Etcher, Solid State Design) [41].

Sterilization of the dishes was carried out for 30 min with the use of UV rays at a power of 15 W in a laminar chamber type II safety class DONSERV LA2-5A1-E type.

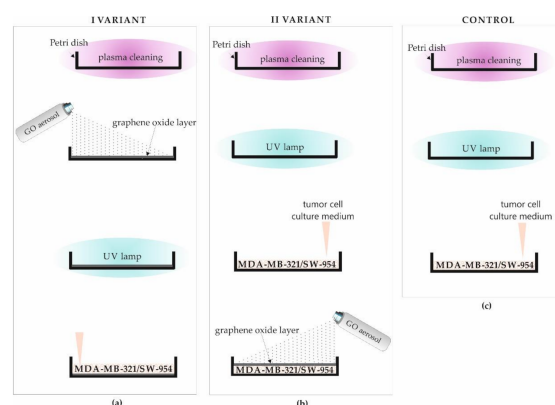


**Figure 1.** Scheme of preparation of Petri dishes for cancer cell culture in: (a) I VARIANT—Petri dish plasma cleaning, GO deposition, sterilization of the Petri dish surface with a UV lamp, and cells culturing; (b) II VARIANT—Petri dish plasma cleaning, sterilization of the Petri dish surface with a UV lamp, cell culturing, and GO deposition; (c) CONTROL—Petri dish plasma cleaning, sterilization of the Petri dish surface with UV lamp, and cells culturing.

### 2.1. Materials

GO flakes (Figure 2) dispersed in water were obtained from flake graphite by a modified Hummers method (Department of Chemical Synthesis and Flake Graphene, Łukasiewicz Research Network—Institute of Electronic Materials Technology, Warsaw, Poland). The average GO thickness was 3–4 layers (around 1.0–1.5 nm) and flake size was 3–10  $\mu\text{m}$ , and the oxygen content was 45–52% [42]. Flake graphite (Asbury Carbons, Asbury, NJ, USA) was added to a reactor containing concentrated sulfuric acid ( $\text{H}_2\text{SO}_4$ , Chempur, Piekary Śląskie, Poland) and phosphoric acid ( $\text{H}_3\text{PO}_4$ , Chempur, Piekary Śląskie, Poland). Next, potassium permanganate ( $\text{KMnO}_4$ , Chempur, Piekary Śląskie, Poland) was slowly added to this mixture. The oxidation process was performed for a few hours and stopped by the addition of deionized water and hydrogen peroxide (30%  $\text{H}_2\text{O}_2$ , Chempur, Piekary Śląskie, Poland). The graphite oxide water suspension obtained was left for sedimentation. Then, the purification and exfoliation processes were performed. The concentration of GO water dispersion was 10 g/L.

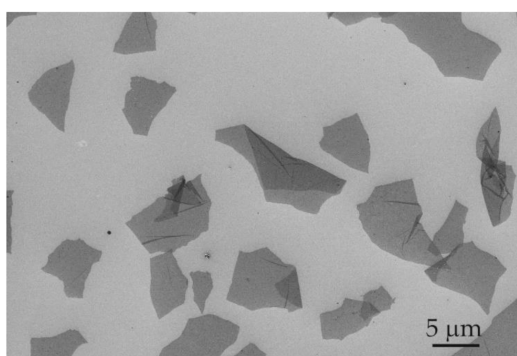


Figure 2. SEM images of GO flakes.

### 2.2. GO Aerosol

A GO aerosol was made according to Bag-On-Valve technology (BOV), which allows the application of the suspension of GO in the form of aerosol without propellant gas contact. An aerosol valve BOV Crimper type was connected with a bag made of four-layered foil (polyethylene, aluminum, nylon, and polypropylene). The set included an Under-The-Cup pre-gassing (UTC) part and a BOV valve locking the aluminum container. Sealing the container allowed air to be applied pressure ranging from 1 to 3 bars between pouch and container. In a further step, the pouch was filled with GO suspension up to 9 bars. The aerosol set was equipped with a valve and spray applicator from Aptara. Spraying strength was regulated with air pressure and the applicator nozzle type. The application time of GO on the Petri dish (variant I) and cells (variant II) was the same, so we conclude that the concentration of GO (10 g/L) is identical in both variants.

### 2.3. Cell Culture

The cell lines (MDA-MB-231 and SW-954) used in this study were obtained from the American Type Culture Collection (ATCC) in Manassas, VA, USA.

Experiments concerning the interaction of GO on cancer cells were carried out with the use of two cancer cell lines, i.e., MDA-MB-231 and SW-954. Cancer cells of the MDA-MB-231 line come from a triple-negative breast cancer characterized by a lack of estrogen, progesterone, and HER2 receptors. Cells were cultivated in Falcon T25 cell culture flasks in the presence of Dulbecco's Minimum Essential Medium Eagle (DMEM) cell culture medium enriched with a 10% fetal bovine serum (FBS) with the addition of selected antibiotics (penicillin/streptomycin). Cancer cells of the SW-954 vulva squamous cell cancer line were cultivated with the use of a L-15 (Leibovitz) medium in the presence of 20% fetal bovine serum (FBS) and antibiotics (penicillin/streptomycin). Both cell lines were cultured under sterile conditions in the incubator in humid conditions containing 5%  $\text{CO}_2$ /95% air (MDA-MB-231) and 100% air (SW-954).

In order to obtain cancer cells for the tests described in the paper, a cancer cells line passage procedure was conducted. First, the cell culture medium was poured out, then the cells were rinsed with PBS without  $\text{Ca}^{2+}$  and  $\text{Mg}^{2+}$  ions and treated with 0.25% trypsin solution. After separation of cells from the cell culture flask surface, a medium with serum was added to the cell culture flask in order to inactivate the trypsin. The content of the cell culture flask was transferred to a 15 mL test tube and centrifuged ( $\text{RCF} = 300 \times g$  for 5 min ( $4\text{ }^\circ\text{C}$ )). After that, the supernatant was removed, and the residue was suspended in a fresh medium and used for further tests.

#### 2.4. Cell Viability Test

A cancer cell viability test was carried out with the use of trypan blue. The test is based on the use of the natural properties of the cell membrane as barriers for compounds with an anionic nature. Anionic compounds (dyes) do not penetrate living cells due to the negative charge of the cell membrane. In the case of permanent damage to the cell membrane, which takes place after the death of the cell, the membrane potential disappears, which in turn allows the penetration of anionic substances into the cell and staining of the cytoplasm or nucleus.

First, the cells were passaged on Petri dishes. The medium from the above the cells was poured out into Eppendorf tubes and then, the cells were rinsed with warm PBS without  $\text{Ca}^{2+}$  and  $\text{Mg}^{2+}$  ions. The cells were separated from the Petri dishes by treating them with a trypsin solution, which was subsequently inactivated with the medium from Eppendorf tubes. Next, the cells were centrifuged ( $\text{RCF} = 300 \times g$  for 5 min) and the cellular pellet was suspended in 300  $\mu\text{L}$  of fresh medium. Then, a mixture consisting of 10  $\mu\text{L}$  of the cell's suspension and 10  $\mu\text{L}$  of 0.2% solution of trypan blue was incubated for 2 min and placed in a Bürker chamber in order to calculate the number of living cells.

Cells of MDA-MB-231 and SW-954 cancer lines (in both variants) were cultured in the incubator in  $37\text{ }^\circ\text{C}$  under humid conditions containing 5%  $\text{CO}_2$ /95% air (MDA-MB-231) and 100% air (SW-954).

The changes in cell viability for variants I and II in comparison with the control samples were presented as percentages. For statistical purposes, cell cultures were replicated 9 times for each cell line, exposure time, and variant.

#### 2.5. FTIR Measurements

Measurements of absorption spectra of GO in the infrared range were made using the FTIR-ATR technique. The measurements were made to confirm GO deposition on the Petri dish surface. For ATR measurements, a Thermo Scientific IS50 ATR Module (ThermoFisher SCIENTIFIC, Waltham, MA, USA) was used. Diamond crystal with incident light radiation at  $45^\circ$  was applied. Spectra were recorded three times each with 126 scans in a range of  $4000\text{--}650\text{ cm}^{-1}$  with a resolution of  $4\text{ cm}^{-1}$ .

#### 2.6. Sample Preparation for Imaging by Scanning Electron Microscopy

For analysis of the surface of the Petri dish, GO deposition characteristics, and collection of the images of cancer cell lines, a Scanning Electron Microscopy (SEM) was used (Quanta 250 FEG SEM, FEI, Hillsboro, OR, USA). In order to improve the conductivity and the quality of SEM images of cancer cells, the samples were dried in a vacuum dryer VacuCell 22 L (BMT Medical Technology s.r.o., Brno-Zábrdovice, Czech Republic) and afterwards, deposited with a 5.04 nm layer of gold with the use of a high vacuum sputtering EM ACE 600. During sputtering, the microscope table rotated under  $120^\circ$ . The gold layer acted not only as a conductor but also provided a protective layer against damage from the electron beam. A SEM image was acquired using a backscattered detector (ETD-BSE, FEI, Hillsboro, OR, USA) with an accelerating voltage of 5 kV for GO and 10 kV for cancer cells (all variants). SEM images analysis established the kind and range of the damage that arose as an interaction between cells and GO aerosol.

### 2.7. Characterization of Cancer Cells by Optical Microscopy

Microscopic observations (mag. 100 and 1000) of the surface morphology were carried out every 24, 48, and 72 h with the use of an optical microscope to assess the influence of GO on the cancer cell morphology. In addition to the assessment of the effect of GO on the morphology of tumor cells, vitality tests were also performed to determine the effect of GO in both variants on the vitality of cells. Performing the viability test allowed the natural state of the cell membrane to be determined and the metabolic state of the cells to be measured, which indicates the potential ability of cells to grow, divide, and metabolize.

### 2.8. Confocal Microscopy

The measurements of the changes in surface roughness as a result of plasma cleansing, UV light interaction, and GO deposition were made using a confocal microscope Zeiss LSM 700 (Carl Zeiss Microscopy, Jena, Germany). The experimental parameters were laser wavelength 405 nm, pinhole 0,5 AU, and gain 416. Ten measurements for each sample were made.

## 3. Results and Discussions

### 3.1. Surface Morphology

The main reason for plasma cleansing was to prepare the surface for GO deposition. This process allowed GO to strongly adsorb on the Petri dish surface [43] and minimized the peeling back of GO flakes during cell culturing. Vacuum drying was applied to reduce the air leftovers trapped between the Petri dish surface and GO layer.

Since other forms of sterilization could considerably influence the GO structure or even peel it off completely, sterilization with UV light was applied. Both processes (drying and sterilization) were carried out to preserve and sterilize the surface of the Petri dish with GO layers and prepare it for the next steps of the experiments.

Figure 3 compares the Petri dish topography before (Figure 3a) and after (Figure 3b) plasma cleansing, and after UV sterilization (Figure 3c) and GO aerosol deposition (Figure 3c). Reduction in contamination was observed on the surface of the Petri dish after plasma cleansing and UV sterilization (Figure 3a–c).

Figure 3e shows the changes after vacuum dryer usage and Figure 3f shows the influence of UV radiation on GO deposited on the Petri dish.

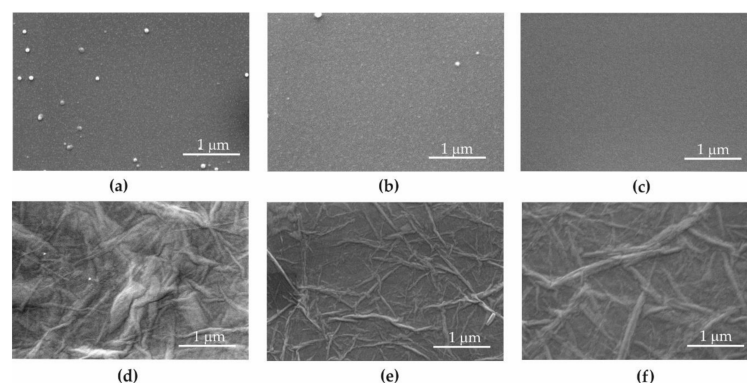


**Figure 3.** SEM images of the surface. (a) Unmodified Petri dish; (b) after plasma cleansing; (c) plasma cleansing and UV sterilization; (d) plasma cleansing and GO deposition; (e) plasma cleansing, GO deposition, and vacuum dryer; (f) plasma cleansing GO deposition, vacuum dryer, and UV sterilization.

As a result of GO deposition in aerosol form, the flake edges overlapped with each other and the bottom of the Petri dish was covered with GO at a level of 100%. Typical characteristics for GO

unevenness of the surface were recorded (Figure 3d). The deposition of GO caused an increase in surface roughness <15% (Table 1).

**Table 1.** Petri dish surface roughness changes (mean out of 10 measurements) with standard deviation.

Surface Type	Mean Value Ra <sup>1</sup> [μm]	Mean Value Rz <sup>2</sup> [μm]
Petri dish surface	0.590 ± 0.04	2.88 ± 0.65
Petri dish surface after plasma cleansing	0.796 ± 0.14	3.25 ± 0.76
Petri dish surface after plasma cleansing and UV sterilization	0.690 ± 0.18	2.74 ± 0.22
Petri dish surface after plasma cleansing and GO deposition	0.848 ± 0.12	2.89 ± 0.28
Petri dish surface after plasma cleansing, GO deposition and vacuum drying	0.984 ± 0.32	4.14 ± 0.36
Petri dish surface after plasma cleansing, vacuum drying and UV sterilization	0.896 ± 0.29	3.85 ± 0.34

<sup>1</sup> Ra—arithmetic average.<sup>2</sup> Rz—maximum peak to valley height of the profile.

In order to confirm the structure of GO after the drying process and sterilization, a FTIR spectrum was recorded (Figure 4). Analysis of the spectrum showed typical absorption bands characteristic for GO.

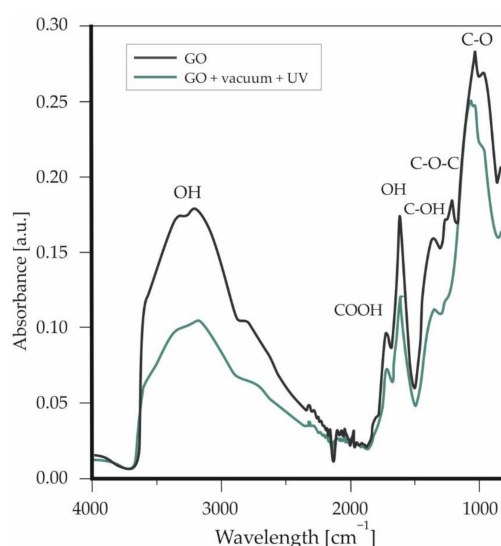


**Figure 4.** FTIR spectrum of GO deposited on the Petri dish.

In a range of 3550–3200  $\text{cm}^{-1}$ , stretching vibrations originating from OH groups can be observed. The band at 1730  $\text{cm}^{-1}$  was assigned to the carboxyl group; 1619  $\text{cm}^{-1}$  corresponds to the stretching and bending vibration of OH groups of water molecule adsorbed on GO. The peak at 1365  $\text{cm}^{-1}$  arises from C–OH, 1225  $\text{cm}^{-1}$ , and denotes C–O–C stretching, and 1047  $\text{cm}^{-1}$  was assigned to C–O vibrations. The GO spectrum after vacuum drying and UV did not differ drastically from the GO spectrum recorded before these processes. Loss in OH groups is visible through the whole spectrum. This may be the effect of water evaporation from the GO or slight reduction in other OH (along with COOH) groups located in GO structure.

### 3.2. Microscopic Analysis of Cancer Cells

Both cell lines were characterized by a different morphology and growth rate. MDA-MB-231 cells grew faster and the cells were not only larger and more branched but also had longer protrusions than the SW-954 cells.

The SW-954 cells were smaller and more compact than the MDA-MB-231 cells. In both cases (variant I—Figures 5a–c and 6a–c; variant II—Figures 5d–f and 6d–f), it was noticeable that there was a clear difference between the GO-treated cells and the control cells (control—Figure 5g–i, Figure 6g–i). In the case of variant I for the MDA-MB-231 cell line, we did not observe significant inhibition of cell count along with the increasing incubation time with GO as compared to the control.

While a microscopic analysis of the SW-954 cell line treated with GO in variant I reveals a decreasing number of cells with increasing incubation time, this may indicate the effect of GO on the count of cancer cell lines. On the other hand, microscopic observation of the results from variant II indicated that GO slightly inhibits cells number and changes the morphology of SW-954 cells after 24, 48, and 72 h incubation, respectively, while no significant effect of GO on the cell count and morphology of MDA-MB-231 cells was noticed. Analysis of the cancer cell structure demonstrated a tendency towards a cytotoxic influence of graphene flakes on the cancer cell lines.

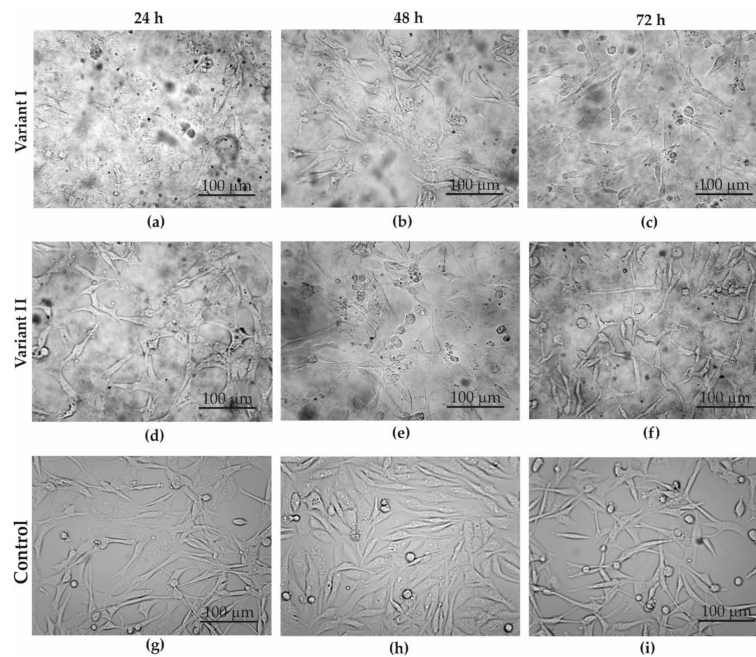


**Figure 5.** Optical microscope images of MDA-MB-231 cell culture in: (a–c) variant I; (d–f) variant II; (g–i) control; after: 24 (a,d,g), 48 (b,e,h), and 72 h (c,f,i).

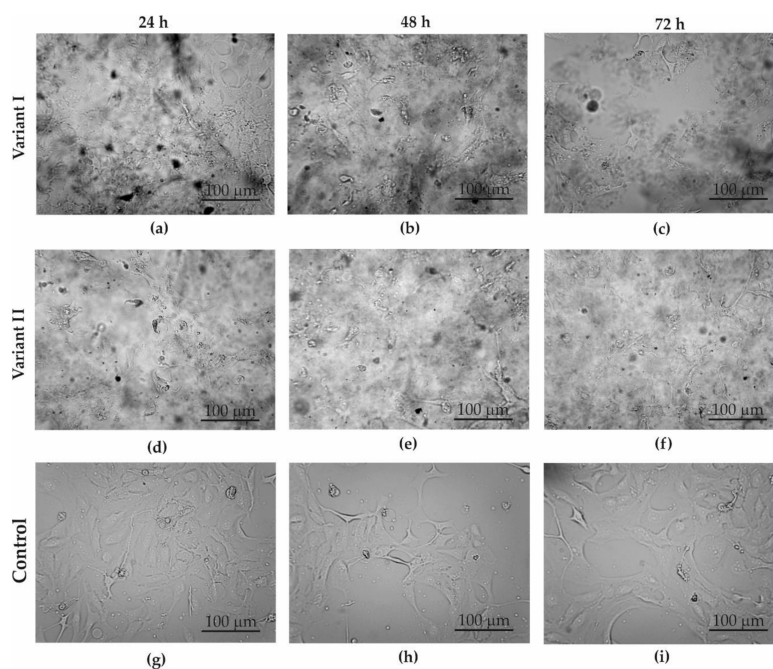


**Figure 6.** Optical microscope images of SW-954 cell culture in: (a–c) variant I; (d–f) variant II; (g–i) control; after: 24 (a,d,g), 48 (b,e,h), and 72 h (c,f,i).

With a SEM analysis, it was observed that all cells treated with the GO aerosol (variant I—Figures 7a–c and 8a–c; variant II—Figures 7d–f and 8d–f) showed surficial deformation of the cell membrane.

While analyzing variant II, when the cancer cells were covered with GO, it was clearly observed that the graphene flakes precipitated on the surface of the cell membrane (Figure 8a). It was observed that right after deposition between the cell membrane and graphene (similar to the case of dead cancer cells), strong adhesive bonds cannot be observed. However, after 24–72 h of interaction with GO, cell morphology was characterized by constricted cell membranes (Figure 8b,c). GO adheres to the cells and covers them hermetically. After 72 h, the GO layer started to break due to strong adhesive forces between the cells and GO. Shrinking cells increased surface tension and caused GO cracks around cells (Figure 7f, Figure 8f).

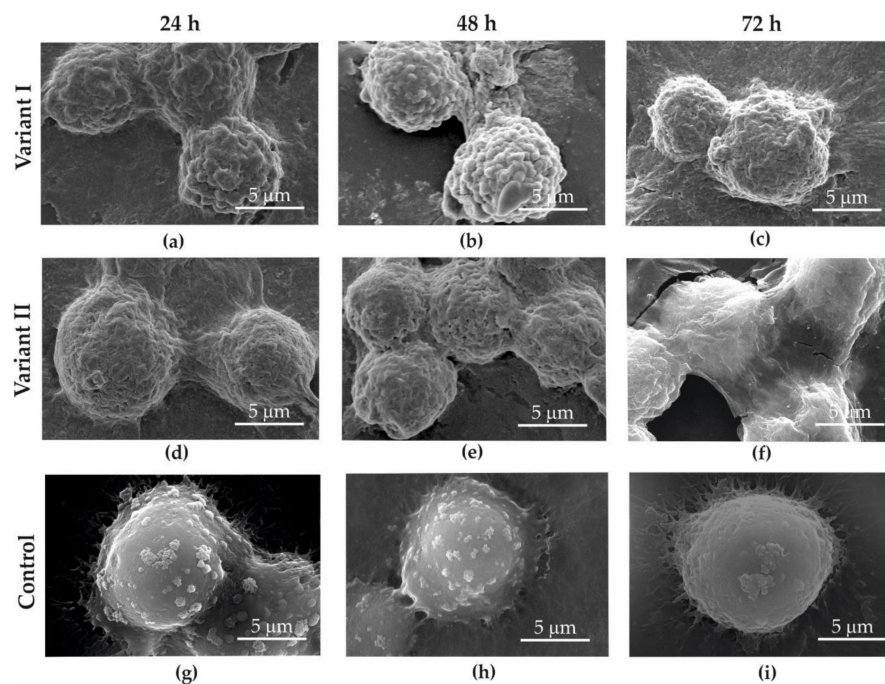


**Figure 7.** SEM image of MDA-MB-231 cancer cells obtained for variant I (a–c); variant II (d–f); control (g–i); after 24 (a,d,g), 48 (b,e,h), and 72 h (c,f,i).

Deformation of the cell membrane was not observed in control samples (control Figures 7g–i and 8g–i), where GO did not interact with the examined cell lines.

Analysis of the SEM images showed that in variant II, a decrease in cell diameter and shrinking of the cell membrane was observed as a result of the GO interaction with cells. GO on the cell surface probably creates a barrier layer which cuts the cells off (partially or totally) from nutrients. It was also observed that after 72 h of incubation in variant II, the surface of GO began to crack and became loose.

When coming into contact with cells, GO twines them and causes surface deformation. The degree of deformation might depend on the time of the interaction, cell age, and the number of graphene flakes influencing the cell membrane.

It is very interesting that the changes in surface morphology of the cancer cells concern only the living cells. In the case where cells were already dead before GO deposition, no changes in cell morphology were observed. This was clearly visible with MDA-MB-231 cells (Figure 9).

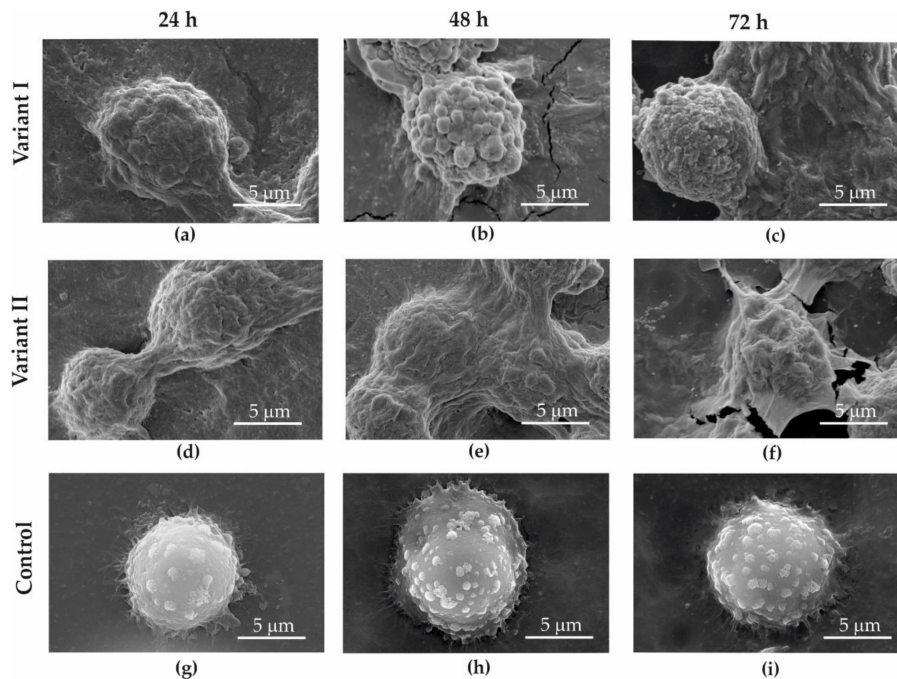


**Figure 8.** SEM image of SW-954 cancer cells obtained for variant I (a–c); variant II (d–f); and control (g–i); after 24 (a,d,g), 48 (b,e,h), and 72 h (c,f,i).

SEM image analysis in variant I showed that the morphology of the cell membrane of the living cell with GO deposited on its surface (Figure 9a) differs in surface development as compared to the surface of cells that were dead before deposition or that died right after deposition (Figure 9b,c). Those cells showed a smooth surface under the GO layer.

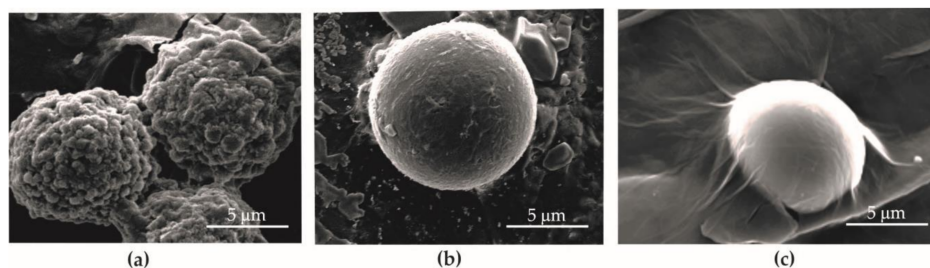


**Figure 9.** SEM images in variant I of MDA-MB-231 cancer cells with GO deposited on: (a) living cells and (b,c) dead.

### 3.3. Cells Viability

A biological viability test with the use of trypan blue showed that cancers cells coated with GO were characterized by reduced viability compared to the control sample and cells cultured on a Petri dish coated with GO. The test showed reduced viability after 72 h in variant I for around 4.3% for both cell lines as compared to the control samples (Figure 10). For variant II, the differences in viability were significantly higher and were 52.7% for MDA-MB-231 and 26.4% for SW-954, respectively (Figure 11). The results presented in Figures 10 and 11 are shown with standard deviation calculated from nine measurements.

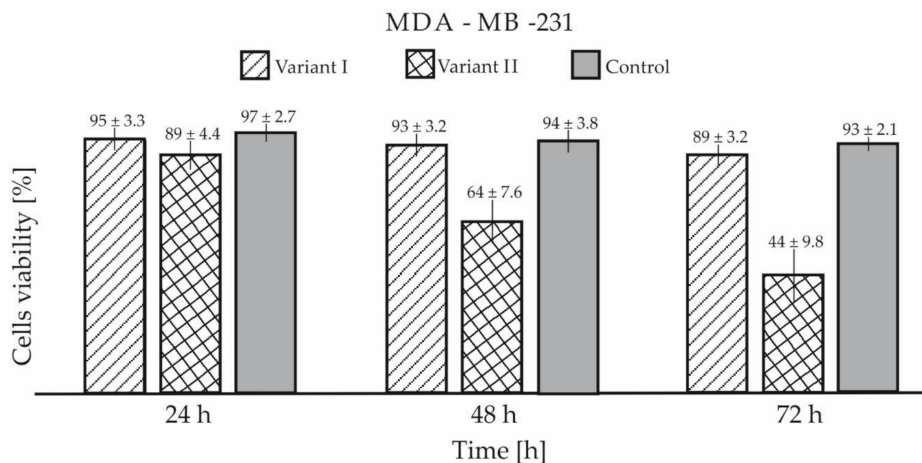


**Figure 10.** Cell viability of MDA-MB-231 in both tested variants.

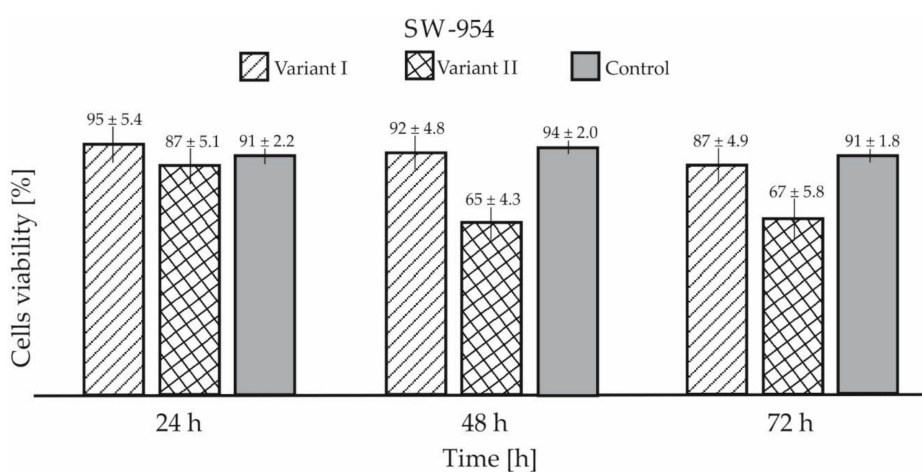


**Figure 11.** Cell viability of SW-954 in both tested variants.

#### 4. Conclusions

In this paper presented, the influence of GO on the biological viability of triple-negative breast cancer and vulva cancer cells was examined. The manner of GO deposition during cell culturing was the factor that drew the authors' attention. Two variants were examined: (I) cells were grown on a GO layer and (II) cells were covered with a GO layer. The results presented were compared to the control samples. The experiments were conducted in the same conditions (temperature, time of culturing, and culturing environments) but the location of the GO was the factor that had a crucial effect on cells. The viability of cells covered with GO (variant II) was lower for 52.7% for MDA-MB-231 and 26.4% for SW-954 lines as compared with the control samples. Cells cultured on a GO layer (variant I) showed a drop in viability of 4.3%, which suggests a scant effect of GO on the cells. This feature was similar for both tested cell lines. It is also possible that the GO layer acts as a barrier for trypan blue and does not allow the dye to react with cells. We cannot rule out the possibility that the viability results are lower than in reality and the cell count would be in fact higher. In addition, morphological changes among these cells were similar. Visible deformations of the shape of the cells were observed in samples with GO. At this point, it is difficult to assess if GO penetrates inside the cells or interacts with the cell membrane, thus impacting cell shape and viability. It is also possible that the drop in viability in variant II was an effect of GO covering the cells. GO, by adhering to the cell membrane, limited the passage of nutrients which caused a decrease in their viability.

It was observed that right after deposition (similar to the case of dead cancer cells) between the cell membrane and graphene, strong adhesive bonds cannot be observed. However, after 24–72 h of interaction with GO, cell morphology is characterized by constricted cell membranes.

GO deposition in the form of aerosol has never been performed before. Some of the issues that arose during the experiments presented require further investigation and will be tackled in the future. These will include the interaction of normal cells with GO aerosol. A comparison of the results of such experiments will allow it to be established whether a GO aerosol possesses anticancer properties.

**Author Contributions:** Conceptualization, B.N. and Z.B.; methodology, B.N., K.H., Z.M., S.G., M.D., A.B., A.K., K.K.; formal analysis, B.N.; investigation, B.N.; resources, B.N.; writing—original draft preparation, B.N.; writing—review and editing, B.N., K.H., A.B., A.K.; visualization, B.N., K.H., A.B.; supervision, B.N., Z.B. All authors have read and agreed to the published version of the manuscript.

**Funding:** This research received no external funding.

**Acknowledgments:** The authors would like to give thanks to Janusz Buchta for technical support during GO aerosol preparation.

**Conflicts of Interest:** The authors declare no conflict of interest.

## References

1. The Nobel Prize. Available online: <https://www.nobelprize.org/prizes/physics/2010/press-release> (accessed on 18 June 2020).
2. Son, H.G.; Oh, H.O.; Park, Y.S.; Kim, D.H.; Lee, D.S.; Park, W.H.; Kim, H.J.; Cho, S.M.; Lim, K.M.; Song, K.S. Micro cell array on silicon substrate using graphene sheet. *Mater. Lett.* **2017**, *196*, 385–387. [[CrossRef](#)]
3. Luo, H.; Sui, Y.; Qi, J.; Meng, Q.; Wei, F.; He, Y. Copper matrix composites enhanced by silver/reduced graphene oxide hybrids. *Mater. Lett.* **2017**, *196*, 354–357. [[CrossRef](#)]
4. Liu, Y.; Zhang, M.; Liu, Y.; Xue, M.; Li, B.; Tao, X. Novel Li<sub>3</sub>VO<sub>4</sub>/MoS<sub>2</sub> composite materials with high electrochemical performance as anode for lithium ion batteries. *Mater. Lett.* **2017**, *196*, 209–212. [[CrossRef](#)]
5. Lv, Q.; Sun, H.; Li, X.; Xiao, J.; Xiao, F.; Liu, L.; Luo, J.; Wang, S. Ultrahigh capacitive performance of three-dimensional electrode nanomaterials based on  $\alpha$ -MnO<sub>2</sub> nanocrystallines induced by doping Au through Å-scale channels. *Nano Energy* **2016**, *21*, 39–50. [[CrossRef](#)]
6. Jensen, C.D.; Lewinski, N.A. Nanoparticle synthesis to green informatics frameworks. *Curr. Opin. Green Sustain. Chem.* **2018**, *12*, 117–126. [[CrossRef](#)]
7. Yin, S.; Zhang, Z.; Ekoi, E.J.; Wang, J.J.; Dowling, D.P.; Nicolosi, V.; Lupoi, R. Novel cold spray for fabricating graphene-reinforced metal matrix composites. *Mater. Lett.* **2017**, *196*, 172–175. [[CrossRef](#)]
8. Fernández-García, L.; Pérez-Mas, A.M.; Álvarez, P.; Blanco, C.; Granda, M. Morphological changes in graphene materials caused by solvents. *Colloids Surf. A Physicochem. Eng. Asp.* **2018**, *558*, 73–79. [[CrossRef](#)]
9. Ma, Y.; Han, J.; Wang, M.; Chen, X.; Jia, S. Electrophoretic deposition of graphene-based materials: A review of materials and their applications. *J. Mater.* **2018**, *4*, 108–120. [[CrossRef](#)]
10. Tabish, T.A. Graphene-based materials: The missing piece in nanomedicine? *Biochem. Bioph. Res. Co.* **2018**, *504*, 686–689. [[CrossRef](#)]
11. García, G.; Pastor, E.; Rivera, L.M. Novel graphene materials for the oxygen reduction reaction. *Curr. Opin. Electrochem.* **2018**, *9*, 233–239.
12. Bourque, A.J.; Rutledge, G.C. Heterogeneous nucleation of an n-alkane on graphene-like materials. *Eur. Polym. J.* **2018**, *104*, 64–71. [[CrossRef](#)]
13. Nasiłowska, B.; Bogdanowicz, Z.; Sarzyński, A.; Skrzeczanowski, W.; Djas, M.; Bartosewicz, B.; Jankiewicz, B.J.; Lipińska, L.; Mierczyk, Z. The influence of laser ablation parameters on the holes structure of laser manufactured graphene paper microsieves. *Materials* **2020**, *13*, 1568.
14. Lavin-Lopez, M.P.; Valverde, J.L.; Ordoñez-Lozoya, S.; Paton-Carrero, A.; Romero, A. Role of inert gas in the CVD-graphene synthesis over polycrystalline nickel foils. *Mater. Chem Phys.* **2019**, *222*, 173–180. [[CrossRef](#)]
15. Kunioishi, N.; Hagino, S.; Fuwa, A.; Yamaguchi, K. Novel pathways for elimination of chlorine atoms from growing Si(100) surface in CVD reactors. *Appl. Surf. Sci.* **2018**, *441*, 773–779. [[CrossRef](#)]
16. Mukanova, A.; Tussupbayev, R.; Sabitov, A.; Bondarenko, I.; Bakenov, Z. CVD graphene growth on a surface of liquid gallium. *Mat. Today* **2017**, *4*, 4548–4554. [[CrossRef](#)]
17. Zhou, W.; Long, Y. Mechanical properties of CVD-SiC coatings with Si impurity. *Ceram. Int.* **2018**, *44*, 21730–21733. [[CrossRef](#)]

18. Kim, D.Y.; Sinha-Ray, S.; Jung-Jae, P.; Jong-Gun, L.; You-Hong, C.; Sang-Hoon, B.; Jong-Hyun, A.; Jung, Y.C.; Kim, S.M.; Yarin, A.L.; et al. Self-Healing Reduced Graphene Oxide Films by Supersonic Kinetic Spraying. *Adv. Funct. Mater.* **2014**, *24*, 4986–4995. [[CrossRef](#)]
19. Xi, W.; Ding, W.; Yu, S.; Lin, N.; Meng, T.; Guo, Q.; Liu, X.; Liu, X. Corrosion behavior of TaC/Ta composite coatings on C17200 alloy by plasma surface alloying and CVD carburizing. *Surf. Coat. Technol.* **2019**, *359*, 426–432. [[CrossRef](#)]
20. Nasiłowska, B.; Bogdanowicz, Z.; Wojucki, M.; Bartosewicz, B.; Djas, M. Corrosion Protection for S235 JR Steel with Graphene Oxide. In Proceedings of the 12th International Scientific Conference Intelligent Technologies in Logistics and, Mechatronics Systems (ITELMS'2018), Panevezys, Lithuania, 26–27 April 2018; pp. 213–218.
21. Deka, M.J.; Chowdhury, D. Surface charge induced tuning of electrical properties of CVD assisted graphene and functionalized graphene sheets. *J. Mater. Sci. Technol.* **2019**, *35*, 151–158. [[CrossRef](#)]
22. Liu, C.; Liu, Z.; Wang, B. Modification of surface morphology to enhance tribological properties for CVD coated cutting tools through wet micro-blasting post-process. *Ceram. Int.* **2018**, *44*, 3430–3439. [[CrossRef](#)]
23. Khan, M.; Khan, M.; Al-Marri, A.H.; Al-Warthan, A.; Alkhatlan, H.Z.; Siddiqui, M.R.H.; Nayak, V.L.; Kamal, A.; Adil, S.F. Apoptosis inducing ability of silver decorated highly reduced graphene oxide nanocomposites in A549 lung cancer. *Int. J. Nanomed.* **2016**, *11*, 873–883.
24. Pereyra, J.Y.; Cuello, E.A.; Salavagione, H.J.; Barbero, C.A.; Acevedo, D.F.; Yslas, E.I. Photothermally enhanced bactericidal activity by the combined effect of NIR laser and unmodified graphene oxide against *Pseudomonas aeruginosa*. *Photodiagn. Photodyn.* **2018**, *24*, 36–43. [[CrossRef](#)] [[PubMed](#)]
25. Sengupta, I.; Bhattacharya, P.; Talukdar, M.; Neogi, S. Bactericidal effect of graphene oxide and reduced graphene oxide: Influence of shape of bacteria. *J. Colloid. Interf. Sci.* **2018**, *528*, 389–399. [[CrossRef](#)]
26. Pinto, A.M.; Gonçalves, I.C.; Magalhães, F.D. Graphene-based materials biocompatibility: A review. *Colloids Surf. B* **2013**, *111*, 188–202. [[CrossRef](#)]
27. Akhavan, O.; Ghaderi, E. Toxicity of graphene and graphene oxide nanowalls against bacteria. *ACS Nano* **2010**, *4*, 5731–5736. [[CrossRef](#)]
28. Jaworski, S.; Sawosz, E.; Grodzik, M.; Winnicka, A.; Prasek, M.; Wierzbicki, M.; Chwalibog, A. In vitro evaluation of the effects of graphene platelets on glioblastoma multiforme cells. *Int. J. Nanomed.* **2013**, *8*, 413–420.
29. Tabish, T.A.; Pranjol, M.Z.I.; Horsell, D.W.; Rahat, A.A.M.; Whatmore, J.L.; Winyard, P.G.; Zhang, S. Graphene Oxide-Based Targeting of Extracellular Cathepsin D and Cathepsin L As A Novel Anti-Metastatic Enzyme Cancer Therapy. *Cancers* **2019**, *11*, 319. [[CrossRef](#)]
30. Wang, X.; Zhou, W.; Li, X.; Ren, J.; Ji, G.; Du, J.; Tian, W.; Liu, Q.; Hao, A. Graphene oxide suppresses the growth and malignancy of glioblastoma stem cell-like spheroids via epigenetic mechanisms. *J. Transl. Med.* **2020**, *18*, 1–14. [[CrossRef](#)]
31. Pei, X.; Zhu, Z.; Gan, Z.; Chen, J.; Zhang, X.; Cheng, X.; Wan, Q.; Wang, J. PEGylated nano-graphene oxide as a nanocarrier for delivering mixed anticancer drugs to improve anticancer activity. *Sci. Rep.* **2020**, *10*, 1–15. [[CrossRef](#)]
32. Liao, C.; Li, Y.; Chin Tjong, S. Graphene Nanomaterials: Synthesis, Biocompatibility, and Cytotoxicity. *Int. J. Mol. Sci.* **2018**, *19*, 3564. [[CrossRef](#)]
33. Nasiłowska, B.; Kowalik, A.; Bogdanowicz, Z.; Sarzynski, A.; Hincza, K.; Gruszynski, K.; Woluntarski, M.; Mierczyk, Z.; Gózdź, S. Application of graphene paper laser ablation for separation of cancer cells. In Proceedings of the Laser Technology 2018: Progress and Applications of Lasers, Jastarnia, Poland, 4 December 2018; Volume 10974, p. 10974.
34. Hu, Y.; Li, F.; Han, D.; Niu, L. Graphene in Drug Delivery, Cellular Imaging, Bacteria Inhibition, Versatile Targets Bioassays. In *Biocompatible Graphene for Bioanalytical Applications*; Springer: Berlin/Heidelberg, Germany, 2014; pp. 103–114.
35. Zhu, Y.; Murali, S.; Cai, W.; Li, X.; Suk, W.; Potts, J.R.; Ruoff, R.S. Graphene and graphene oxide: Synthesis, properties, and applications. *Adv. Mater.* **2010**, *22*, 3906–3924. [[CrossRef](#)] [[PubMed](#)]
36. Li, Y.; Yuan, H.; Bussche, A.; Creighton, M.; Hurt, R.H.; Kane, A.B.; Gao, H. Graphene microsheets enter cells through spontaneous membrane penetration at edge asperities and corner sites. *Prac. Natl. Acad. Sci. USA* **2013**, *110*, 12295–12300. [[CrossRef](#)] [[PubMed](#)]
37. Hu, W.; Peng, C.; Luo, W.; Lv, M.; Li, X.; Li, D.; Huang, Q.; Fan, C. Graphene-based antibacterial paper. *ACS Nano* **2010**, *4*, 4317–4323. [[CrossRef](#)] [[PubMed](#)]

38. Guo, Z.; Xie, C.; Zhang, P.; Zhang, J.; Wang, G.; He, X.; Ma, Y.; Zhao, B.; Zhang, Z. Toxicity and transformation of graphene oxide and reduced graphene oxide in bacteria biofilm. *Sci. Total Environ.* **2017**, *580*, 1300–1308. [[CrossRef](#)] [[PubMed](#)]
39. Fadeel, B.; Bussy, C.; Merino, S.; Vazquez, E.; Flahaut, E.; Mouchet, F.; Evariste, L.; Gauthier, L.; Koivisto, A.J.; Vogel, U.; et al. Safety Assessment of Graphene-Based Materials: Focus on Human Health and the Environment. *ACS Nano* **2018**, *12*, 10582–10620. [[CrossRef](#)]
40. Jaworski, S.; Sawosz, E.; Kutwin, M.; Wierzbicki, M.; Hinzmann, M.; Grodzik, M.; Winnicka, A.; Lipińska, L.; Wlodyga, K.; Chwalibog, A. In vitro and in vivo effects of graphene oxide and reduced graphene oxide on glioblastoma. *Int. J. Nanomed.* **2015**, *10*, 1585–1596.
41. Chang, Y.; Yang, S.T.; Liu, J.H.; Dong, E.; Wang, Y.; Cao, A.; Liu, H.; Wang, H. In vitro toxicity evaluation of graphene oxide on A549 cells. *Toxicol. Lett.* **2001**, *200*, 201–210. [[CrossRef](#)]
42. Shuangli, Y.; Honghua, H.; Cailei, Y.; Feng, L.; Min, Z.; Xinzhi, S.; Chang, Q.; Gaofeng, W. Thickness-Dependent Strain Effect on the Deformation of the Graphene-Encapsulated Au Nanoparticles. *J. Nanom.* **2014**, *2014*, 1–6.
43. Nasiłowska, B.; Olkowicz, K.; Bombalska, A. Surface morphology analysis and wettability of steel and glass modified with graphene oxide. *Proc. Struct. Integ.* **2019**, *16*, 230–236. [[CrossRef](#)]



© 2020 by the authors. Licensee MDPI, Basel, Switzerland. This article is an open access article distributed under the terms and conditions of the Creative Commons Attribution (CC BY) license (<http://creativecommons.org/licenses/by/4.0/>).